

Aging of the 2+1 dimensional Kardar-Parisi-Zhang model

Géza Ódor (1), Jeffrey Kelling (2,3) and Sibylle Gemming (2,3)

(1) MTA TTK MFA Research Institute for Natural Sciences,
P.O.Box 49, H-1525 Budapest, Hungary

(2) Institute of Ion Beam Physics and Materials Research
Helmholtz-Zentrum Dresden-Rossendorf

P.O.Box 51 01 19, 01314 Dresden, Germany

(3) Institute of Physics, TU Chemnitz
09107 Chemnitz, Germany

Extended dynamical simulations have been performed on a 2+1 dimensional driven dimer lattice gas model to estimate ageing properties. The auto-correlation and the auto-response functions are determined and the corresponding scaling exponents are tabulated. Since this model can be mapped onto the 2+1 dimensional Kardar-Parisi-Zhang surface growth, our results contribute to the understanding of the universality class of that basic system.

PACS numbers: 05.70.Ln, 05.70.Np, 82.20.Wt

I. INTRODUCTION

Physical ageing occurring in different systems like glasses, polymers, reaction-diffusion systems or cross-linked networks has been studied in physics systematically since [1]. Ageing occurs naturally in irreversible systems, relaxing towards non-equilibrium stationary states (for a recent comprehensive overview see [2]). In many systems a single dynamical length scale $L(t) \sim t^{1/z}$ describes the dynamics out of equilibrium [3]. In ageing systems the time-translation invariance is broken and they are best characterized by two-time quantities, like the dynamical correlation and response functions [4]. The dynamical scaling laws and exponents describing these functions characterize the non-equilibrium universality classes [5].

In the ageing regime: $s \gg \tau_m$ and $t - s \gg \tau_m$, where τ_m is a microscopic time scale, one expects the following laws

$$C(t, s) = \langle \phi(t)\phi(s) \rangle - \langle \phi(t) \rangle \langle \phi(s) \rangle = s^{-b} f_C \left(\frac{t}{s} \right) \quad (1)$$

$$R(t, s) = \left. \frac{\delta \langle \phi(t) \rangle}{\delta j(s)} \right|_{j=0} = \langle \phi(t) \tilde{\phi}(s) \rangle = s^{-1-a} f_R \left(\frac{t}{s} \right)$$

where s denotes the start and $t > s$ the observation time, j is the external field conjugate to ϕ . These laws define the so-called ageing exponents a, b and the scaling functions, with the asymptotic behavior $f_{C,R}(t/s) \sim (t/s)^{-\lambda_{C,R}/z}$ and the auto-correlation and auto-response exponents $\lambda_{C,R}$, where z is the dynamical exponent.

The KPZ equation describes the evolution of a fundamental non-equilibrium model and exhibits ageing behavior. The state variable is the height function $h(\mathbf{x}, t)$ in the d dimensional space

$$\partial_t h(\mathbf{x}, t) = v + \nu \nabla^2 h(\mathbf{x}, t) + \lambda (\nabla h(\mathbf{x}, t))^2 + \eta(\mathbf{x}, t). \quad (2)$$

Here v and λ are the amplitudes of the mean and local growth velocity, ν is a smoothing surface tension coefficient

and η roughens the surface by a zero-average, Gaussian noise field exhibiting the variance $\langle \eta(\mathbf{x}, t)\eta(\mathbf{x}', t') \rangle = 2T\nu\delta^d(\mathbf{x} - \mathbf{x}')(t - t')$. The letter T is related to the noise amplitude (the temperature in the equilibrium system) and $\langle \rangle$ denotes a distribution average.

The research of this nonlinear stochastic differential equation and universality class introduced by Kardar, Parisi and Zhang (KPZ) [6] is in the forefront of interest nowadays again. [7–12]. This equation was inspired in part by the stochastic Burgers equation [13] and can describe the dynamics of simple growth processes in the thermodynamic limit [15, 16], randomly stirred fluid [14], directed polymers in random media [28] dissipative transport [25, 26], and the magnetic flux lines in superconductors [27]. In one dimension a mapping [42] onto the Asymmetric Exclusion Process (ASEP) [29] exists. In this case the equation is solvable due to the Galilean symmetry [14] and an incidental fluctuation-dissipation symmetry [28]. Recently a progress has been achieved in exact solutions for various one-dimensional realizations and initial conditions (see, for example, Refs. [17–21]).

In higher dimensions only approximations are available. It has been investigated by various analytical [7, 30–32, 36, 37] and numerical methods [9, 34, 35, 38], still there are several controversial issues. Discretized versions of KPZ have been studied a lot in the past decades (for a review see [15]). Recently we have shown [39, 40] the mapping between the KPZ surface and the ASEP [42, 43] can straightforwardly be extended to higher dimensions. In two dimensions the mapping is just the simple extension of the rooftop model to the octahedron model as can be seen on Fig. 2 of [39]. The surface built up from the octahedra can be described by the edges meeting in the up/down middle vertexes. The up edges in the x or y directions are represented by $\sigma_{x/y} = 1$'s, while the down ones by $\sigma_{x/y} = -1$ ' in the model. This can also be understood as a special $2d$ cellular automaton

[44] with the generalized Kawasaki updating rules

$$\begin{pmatrix} -1 & 1 \\ -1 & 1 \end{pmatrix} \frac{p}{q} \begin{pmatrix} 1 & -1 \\ 1 & -1 \end{pmatrix} \quad (3)$$

with probability p for attachment and probability q for detachment. By the lattice gas representation with $n_{x/y} = (1 - \sigma_{x/y})/2$ occupation variables it describes the oriented migration of self-reconstructing dimers. We have confirmed that this mapping using the parametrization: $\lambda = 2p/(p + q) - 1$ reproduces the one-point functions of the continuum model [39, 40].

This kind of generalization of the ASEP model can be regarded as the simplest candidate for studying KPZ in $d > 1$: a one-dimensional model of self-reconstructing d -mers on the d -dimensional space. Furthermore this lattice gas can be studied by very efficient simulation methods. Dynamic, bit-coded simulations were run on extremely large sized ($L \times L$) lattice gas models [40, 41] and the surface heights, reconstructed from the slopes

$$h_{i,j} = \sum_{l=1}^i \sigma_x(l, 1) + \sum_{k=1}^j \sigma_y(i, k) \quad (4)$$

were shown to exhibit KPZ surface growth scaling in $d = 1 - 5$ dimensions.

Recently in $2 + 1$ dimensions Daquila and Täuber [48] have simulated the long-time behavior of the density-density auto-correlation function in driven lattice gases with particle exclusion and periodic boundary conditions in 1-3 spatial dimensions. In one dimension, their model is just the ASEP. They generalized this driven lattice gas model to higher dimensions by keeping the ASEP dynamics in one of the dimensions and performing unbiased random walk in the transverse dimension(s). In two dimensions they reported: $\lambda_C/z = 1$ and $b = -1$. We will show here that our generalization of ASEP model, which exhibits the surface growth scaling of the $2 + 1$ dimensional KPZ model provides different auto-correlation exponents.

Even more recently Henkel et al [47] have determined the ageing exponents of the $1 + 1$ dimensional KPZ equation: $a = -1/3$, $b = -2/3$, $\lambda_C = \lambda_R = 1$ and $z = 3/2$. They solved the discretized KPZ equation (2) in the strong coupling limit [45], or else the Kim-Kosterlitz (KK) model [46]. The KK model uses a height variable $h_i(t) \in \mathbb{Z}$ attached to the sites of a chain with L sites and subject to the constraints $|h_i(t) - h_{i\pm 1}(t)| = 0, 1$, at all sites i .

II. BIT-CODED GPU ALGORITHMS

The height of each surface site is thoroughly determined by two slopes, along the x and y axes respectively, whose absolute values are restricted to unity. Thus at each site two bits of information are required, hence a chunk of 4×4 sites is encoded in one 32-bit word.

Two different layers of parallelization are used that reflect the two layered compute architecture provided by GPUs [54]: not communicating blocks at *device level* and communicating threads at *work-group level*. Parallelization of the algorithm is enabled by splitting the system into spatial domains, which can be updated independently for a limited time without introducing relevant errors. At device layer a domain decomposition scheme using dead borders is employed, see figure 1a. Here conflicts at the subsystem borders are avoided by not updating them. A random translation is applied to the origin of the decomposition periodically. These translations are restricted to multiples of four sites, because 4×4 sites are encoded in one 32-bit word. At work-group level *double tiling* decomposition is employed, see figure 1b. Here the tiles assigned to different work-items are split into 2^d domains. In our two-dimensional problem, this creates 2^2 sets of non-interacting domains, each set consisting of one domain out of every tile. The active set of domains is randomly chosen before each update.

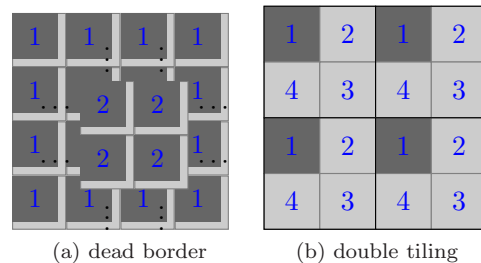


FIG. 1: (Color online) Sketches of the domain decomposition methods used to parallelize the model. Regions that can be updated independently at a time are filled dark-grey. (a) Dead border scheme as used at device level. (b) Double tiling scheme as used at work-group level.

For random number generation, each thread uses a 64-bit linear congruential generator. The threads skip ahead in the sequence, in order to take numbers from disjunct sub-sequences. [53]

A more detailed description of our CUDA implementation can be found in [52]. For this work we added the capability to perform simulations with arbitrary probabilities p and q . Benchmarks, comparing our GPU implementation on a Tesla C2070 to the optimized sequential CPU implementation running on an Intel Xeon X5650 at 2.67 GHz, have shown a speedup-factor of about 230 for the raw simulation. The basic version from [52], which contains less computational effort per update, reaches a raw simulation speedup of about 100, in the same setup.

We decided to not implement space-dependent disorder in our GPU code, because we only need this code for the very small fraction of the computation before the waiting time $s \leq 100$ MCS. Thus the projected benefit regarding time-to-solution would not have justified the effort. Simulations to obtain auto-response calcu-

lations were performed using the CPU code up to the waiting time and then continued on the GPU. The overall speedup-factor obtained by using a GPU in our use-case was about 17. The difference to the number stated above results from using the CPU code until reaching the waiting time and, predominantly, from the computation of the auto-response not being done in parallel. In the auto-correlation runs measurements were performed asynchronously with the simulation, in both CPU and GPU versions. For these runs the gross speedup from using a GPU is about 50.

Applying any kind of domain decomposition to a stochastic cellular automaton introduces an error. This error is kept small by keeping the ratio between the volume of domains and the number of updated sites between synchronization event large as well as by conserving the equidistribution of site-selection as best as possible. The validity of the results was checked primarily by comparing with results obtained with the sequential CPU implementation. For the auto-correlation of slopes we noticed possible signs of saturation below $C_n \lesssim 1 \times 10^{-4}$. This gives an upper limit for the accuracy of our GPU results, independent of statistics. Further investigations suggest, that the above-mentioned restriction of the translations of the decomposition-origin to multiples of four sites may be the sole source of this error. This restriction impairs the equidistribution of site-selection, while not enough to measurably change W^2 scaling, enough to visibly change the auto-correlation behavior of the system. We assume that this problem can be taken care of by removing this restriction in the future.

III. AGING SIMULATIONS

We have run simulations for linear sizes: $L = 2^{12}, 2^{13}, 2^{15}$ of independent samples 30000, 5000, 1000 (respectively), by starting from half filled (striped) lattice gases. The time between measurements increases exponentially

$$t_{i+1} = (t_i + 10) \cdot e^m, \quad \text{with } m > 0, \quad t_0 = 0, \quad (5)$$

when the program calculates the heights $h_{\vec{r}}$ via Eq. (4) at each lattice site $\vec{r} = (i, j)$ and writes out the auto-correlation and the auto-response values to files, which are analyzed later. We used $s = 30, 100, 300$ start times in the two-point function measurements. By simple scaling the morphology of the surface is characterized by the roughness

$$W^2(L, t) = \frac{1}{L^2} \sum_{\vec{r}} \langle (h_{\vec{r}}(t) - \bar{h}(t))^2 \rangle \quad (6)$$

on a lattice with L^2 sites and average height $\bar{h}(t) = L^{-2} \sum_{\vec{r}} h_{\vec{r}}(t)$, which obeys the scaling relation

$$W(L, t) = L^\alpha f(tL^{-z}), \quad f(u) \sim \begin{cases} u^\beta & ; \text{ for } u \ll 1 \\ \text{const.} & ; \text{ for } u \gg 1 \end{cases} \quad (7)$$

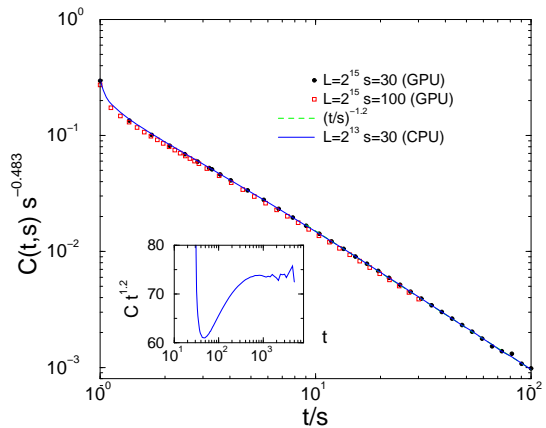


FIG. 2: (Color online) Auto-correlation function scaling of the height variables for $L = 2^{15}$, $s = 30$ (bullets), $s = 100$ (squares) and $L = 2^{13}$, $s = 30$ (line). The dashed line shows a power-law fit for $t/s > 10$ with the slope -1.2 . Inset: The $L = 2^{13}$, $s = 30$ auto-correlation data multiplied by the asymptotic scaling, showing periodic corrections to the decay.

In this form β is the growth exponent and the roughness exponent is $\alpha = \beta z$. Throughout this paper we used the estimates from our previous high precision simulation study [41]: $\alpha = 0.393(4)$, $\beta = 0.2415(15)$ and the dynamical scaling exponent $z = \alpha/\beta = 1.627(26)$.

Similarly to the one-dimensional case we considered here the two-time temporal correlator

$$\begin{aligned} C(t, s) &= \langle (h(t; \vec{r}) - \langle \bar{h}(t; \vec{r}) \rangle) (h(s; \vec{r}) - \langle \bar{h}(s; \vec{r}) \rangle) \rangle \\ &= \langle h(t; \vec{r}) h(s; \vec{r}) \rangle - \langle \bar{h}(t; \vec{r}) \rangle \langle \bar{h}(s; \vec{r}) \rangle \\ &= s^{-b} f_C \left(\frac{t}{s} \right), \end{aligned} \quad (8)$$

where $\langle \rangle$ denotes averaging for sites and independent runs.

The auto-correlation exponent can be read-off in the $(t/s) \rightarrow \infty$ limit: $f_C(t/s) \sim (t/s)^{-\lambda_C/z}$ and since $W^2(t; \infty) = C(t, t) = t^{-b} f_C(1)$ the $b = -2\beta$ relation holds. The simulations were tested by blocking the communication in one of the directions and comparing the results with those of the one dimensional KPZ ageing results [47]. As we found perfect match we believe our two-dimensional results give reliable numerical estimates.

As Fig. 2 shows we could obtain remarkable data collapse for $s = 30$ and $s = 100$ by simulating $2^{15} \times 2^{15}$ sized systems on GPUs. For smaller sizes it is more difficult to reach t/s large, due to the high signal/noise ratio. Least squares error power-law fit for the $t/s > 10$ region gives $C \sim (t/s)^{-1.20(1)}$, however a periodic correction to scaling can also be observed on the inset of Fig. 2. Such oscillations are shown to be the consequence of density fluctuations being transported through a finite system by kinematic waves [40, 55].

In [56] the auto-correlation exponents of the KPZ were

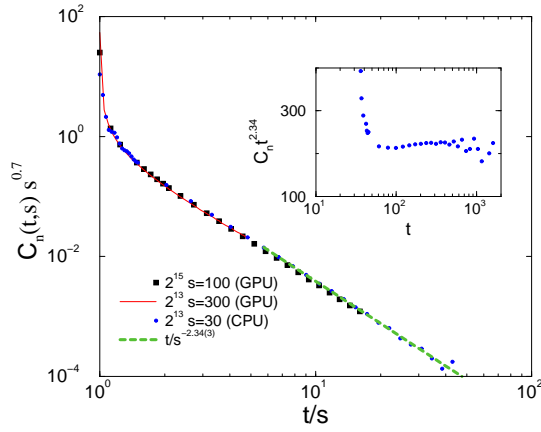


FIG. 3: (Color online) Auto-correlation function scaling of the lattice gas variables for : $L = 2^{15}$ $s = 100$ (boxes, GPU), $L = 2^{13}$, $s = 300$ (line, GPU), $L = 2^{13}$, $s = 30$ (squares, CPU). The dashed line shows a power-law fit: $\sim (t/s)^{-2.34}$ for $t/s > 4$. Inset: The data for $L = 2^{13}$, $s = 30$ is multiplied by the asymptotic scaling.

computed within the dynamic renormalization group (RG) approach. This resulted in $C(\mathbf{q}, t, s) \propto (t/s)^{-1.7}$ scaling in the $2 + 1$ dimensional momentum space. If we transform it to real space we need to integrate the spatial variables as $t^{1/z}$ (where $1/z = 0.614$ in 2d), thus our results agree: $1.7 - (1/z) \simeq 1.2$ fairly well.

We have also calculated the auto-correlation of the density variables

$$\begin{aligned} C_n(t, s) &= \langle (n(t; \vec{r}) - \langle \bar{n}(t; \vec{r}) \rangle) (n(s; \vec{r}) - \langle \bar{n}; \vec{r}(s) \rangle) \rangle \\ &= \langle n(t; \vec{r}) n(s; \vec{r}) \rangle - \langle \bar{n}(t; \vec{r}) \rangle \langle \bar{n}(s; \vec{r}) \rangle \\ &= s^{-b'} f'_C \left(\frac{t}{s} \right), \end{aligned} \quad (9)$$

however, that decays much faster than the height auto-correlator and obtaining reasonable signal/noise ratio requires much higher statistics. This constrained the maximum time we could reach. Still as Fig. 3 shows good data collapse could be achieved with $b' = -0.70(1)$ and $C_n(s, t) \propto (t/s)^{-2.34(3)}$ asymptotically. In fact the height-height and the density-density correlation functions can be related (see [57]) :

$$C_n(\vec{r}, t) \sim \frac{\partial^2}{\partial \vec{r}^2} C(\vec{r}, t), \quad (10)$$

thus a $2/z = 1.228$ difference connects the temporal exponents $\lambda_C/z = 1.20(1)$ and $\lambda_{C_n}/z = 2.34(3)$ indeed.

Next we investigated the scaling of the auto-response function in a similar way as described in [47]. Initially we applied a space-dependent deposition rate $p_i = p_0 + a_i \varepsilon/2$ with $\Delta = \pm 1$ and $\varepsilon = 0.005$ a small parameter. Then later on we used the same stochastic noise η (random sequences), in two realizations. System A evolved, up to

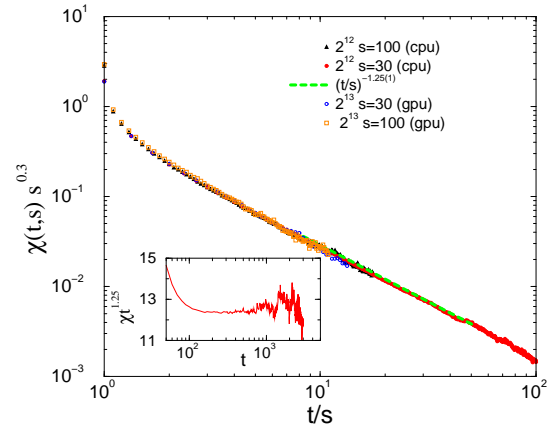


FIG. 4: (Color online) Auto-response function scaling for $L = 2^{12}$ (CPU) $s = 100$ triangles) $s = 30$ dots and $L = 2^{13}$ (GPU) $s = 30$ circles, $s = 100$ squares. The dashed line shows an asymptotic fit $\sim (t/s)^{1.25(1)}$ for the $L = 2^{12}$, $s = 30$ data in the $10 < t/s < 50$ region. Inset: $\chi t^{1.25}$ of the $L = 2^{12}$, $s = 30$ data.

the waiting time s , with the site-dependent deposition rate p_i and afterward, with the uniform deposition rate $p_0 = (1 - q_0) = 0.98$. System B evolved always with the uniform deposition rate $p_i = p_0$. The time-integrated response function is

$$\begin{aligned} \chi(t, s) &= \int_0^s du R(t, u) \\ &= \frac{1}{L^2} \sum_{\vec{r}} \left\langle \frac{h_{\vec{r}}^{(A)}(t, s) - h_{\vec{r}}^{(B)}(t)}{\varepsilon \Delta} \right\rangle = s^{-a} f_\chi \left(\frac{t}{s} \right) \end{aligned} \quad (11)$$

Asymptotically for $(t/s) \rightarrow \infty$ one can read off the auto-response exponent: $f_\chi(y) \sim (t/s)^{-\lambda_R/z}$.

Again, first we tested our programs by comparing the results against the one dimensional KPZ case [47] by restricting the communication among particles to one of the directions. Then we run large scale simulations on CPUs for $L = 2^{12}$ up to 37000 samples and for GPUs for $L = 2^{13}$ up to 37000 samples. Hardware independence was confirmed and a good scaling collapse was achieved by the exponents shown on Fig. 4. Most obvious is that $\lambda_R \neq \lambda_C$, so the fluctuation-dissipation relation $TR(t, s) = -\partial_r^2 C(t, s)$, which is fulfilled in one dimension due to the time-reversal symmetry [14, 37, 50] is broken here. The ageing exponents are different from the 1d KPZ [47] and those of the 2d driven lattice gas model of [48]. They are summarized in table I.

a	b	λ_R	λ_C	β	α
0.30(1)	-0.483(2)	2.03(1)	1.95(1)	0.2415(15)	0.393(4)

TABLE I: Scaling exponents of the $d = 2 + 1$ dimensional KPZ class.

The inset of Fig. 4 shows the corrections to the long-time scaling, suggesting oscillating convergence as in the case of the auto-correlations.

IV. CONCLUSIONS AND DISCUSSION

We have extended our previous, bit-coded 2d driven dimer lattice gas model simulations with auto-correlation and auto-response measurement capability in order to investigate the ageing behavior. This gas can be mapped onto a surface growth (octahedron) model, which exhibits KPZ surface scaling exponents, thus our height auto-correlation and auto-response functions describe the ageing properties of two dimensional KPZ surfaces. By performing extensive simulations both on CPUs and GPUs we have determined the ageing exponents for this universality class. The auto-correlation exponents are different from those of the two-dimensional driven lattice gas [48], however agreement can be found with the RG predictions of [56] for the KPZ. The violation of the fluctuation-dissipation relation is confirmed numerically.

We have also provided numerical estimates for the

auto-correlation exponents for the density variables of the lattice gas. The performance of the GPU code with respect to the CPU algorithm is higher by about a factor of 230. Our method is capable to test numerically predictions of the Local Scale Invariance hypothesis (see [2]) and is straightforwardly extensible to higher dimensions [40].

Acknowledgments:

Support from the Hungarian research fund OTKA (Grant No. K109577), and the OSIRIS FP7 is acknowledged. We thank Karl-Heinz Heinig for initiating the German-Hungarian cooperation and laying the ground for our large scale simulations, Uwe Täuber, Tim Halpin-Healy and Malte Henkel for their useful comments. The authors thank NVIDIA for supporting the project with high-performance graphics cards within the framework of Professor Partnership. Jeffrey Kelling thanks Karl-Heinz Heinig for his mentoring on bit-coded simulations and Bartosz Liedke for additional support in this matter.

-
- [1] L. C. E. Struik, *Physical Aging in Amorphous Polymers and Other Materials* (Elsevier, New York, 1978).
 - [2] M. Henkel and M. Pleimling, *Non-equilibrium phase transitions, vol 2: Ageing and dynamical scaling far from equilibrium*, Springer (Heidelberg 2010).
 - [3] A. J. Bray, *Adv. Phys.* **43**, 357 (1994).
 - [4] L. F. Cugliandolo, in *Slow Relaxation and Non-equilibrium Dynamics in Condensed Matter*, ed.: J.-L. Barrat, J. Dalibard, J. Kurchan, and M. V. Feigelman (Springer, 2003).
 - [5] G. Ódor, *Universality in Nonequilibrium Lattice Systems*, (World Scientific, Singapore, 2008).
 - [6] M. Kardar, G. Parisi, and Y. Zhang, *Phys. Rev. Lett.* **56**, 889 (1986).
 - [7] T. Kloss, L. Canet and N. Wschebor, *Phys. Rev. E* **86** 051124
 - [8] I. Corwin, *Random Matrices: Theory and Applications*, **1** (2012).
 - [9] T. Halpin-Healy, *Phys. Rev. Lett* **109**, 170602 (2012)
 - [10] T. Halpin-Healy, *Phys. Rev. E* **88**, 042118 (2013)
 - [11] J. Olejarz, P. L. Krapivsky, *Phys. Rev. E* **88**, 022109 (2013)
 - [12] M. Nicoli, R. Cuerno, M. Castro, *J. Stat. Mech.* (2013) P11001
 - [13] J. M. Burgers, *The Nonlinear Diffusion Equation*, (Riedel, Boston 1974).
 - [14] D. Forster, *Phys. Rev. A*, **16**, (1977) 732.
 - [15] A. L. Barabási and H. E. Stanley, *Fractal Concepts in Surface Growth*, (Cambridge University Press, Cambridge 1995).
 - [16] T. Halpin-Healy, *Phys. Rev. A* **42**, 711 (1990).
 - [17] K. Johansson, *Comm. Math. Phys.* 209, **437** (2000).
 - [18] M. Prahofer and H. Spohn, *Phys. Rev. Lett.* **84**, 4882 (2000).
 - [19] P. Ferrari, *Comm. Math. Phys.* **252**, 77 (2004).
 - [20] T. Sasamoto, *J. Phys. A* **38**, L549 (2005).
 - [21] P. Calabrese and P. L. LeDoussal, *Phys. Rev. Lett.* **106**, 250603 (2011).
 - [22] T. Halpin-Healy and Y.-C. Zhang, *Phys. Rep.* **254**, (1995) 215.
 - [23] J. Krug, *Adv. Phys.* **46**, (1997) 139.
 - [24] M. Kardar, *Phys. Rev. Lett.* **55**, (1985) 2923
 - [25] H. K. Janssen and B. Schmittmann, *Z. Phys. B*, **63**, (1986) 517.
 - [26] H. van Beijeren, R. Kutner and H. Spohn, *Phys. Rev. Lett.* **54**, (1985) 2056.
 - [27] T. Hwa, *Phys. Rev. Lett.* **69**, (1992) 1552.
 - [28] M. Kardar, *Nucl. Phys. B* **290**, (1987) 582.
 - [29] H. Rost, *Z. Wahrsch. Verw. Gebiete*, **58**, (1981) 41.
 - [30] M. Schwartz and S.F. Edwards, *Europhys. Lett.* **20**, (1992) 301.
 - [31] E. Frey and U. C. Täuber, *Phys. Rev. E*, **50**, (1994) 1024.
 - [32] M. Lässig, *Nucl. Phys. B*, **448** (1995) 559.
 - [33] B. M. Forrest and L. H. Tang, *Phys. Rev. Lett.* **64**, (1990) 1405.
 - [34] E. Marinari, A. Pagnani and G. Parisi, *J. Phys. A* **33**, (2000) 8181.
 - [35] E. Marinari, A. Pagnani, G. Parisi and Z. Rácz, *Phys. Rev. E* **65** (2002) 026136.
 - [36] H. C. Fogedby, *Phys. Rev. Lett.* **94**, (2005) 195702.
 - [37] L. Canet, H. Chat, B. Delamotte, N. Wschebor, *Phys. Rev. E* **84** (2011) 061128.
 - [38] F. D. A AaraoReis, *Phys. Rev. E* **72** (2005) 0322601.
 - [39] G. Ódor, B. Liedke and K.-H. Heinig, *Phys. Rev. E* **79**, (2009) 021125.
 - [40] G. Ódor, B. Liedke and K.-H. Heinig, *Phys. Rev. E* **81**, (2010) 031112.
 - [41] J. Kelling and G. Ódor, *Phys. Rev. E* **84** (2011) 061150

- [42] M. Plischke, Z. Rácz and D. Liu, Phys. Rev. B **35**, (1987) 3485.
- [43] P. Meakin, P. Ramanlal, L. M. Sander and R. C. Ball, Phys. Rev. A **34**, (1986) 5091.
- [44] S. Wolfram, Rev. Mod. Phys. **55**, (1983) 601.
- [45] T. J. Newman and M. R. Swift, Phys. Rev. Lett. **79**, 2261 (1997)
- [46] J. M. Kim and J. M. Kosterlitz, Phys. Rev. Lett. **62**, 2289 (1989).
- [47] M. Henkel, J. D. Noh, M. Pleimling, Phys. Rev. E **85**, 030102(R) (2012).
- [48] G. L. Daquila and Uwe C. Täuber, Phys. Rev. E **83** (2011) 051107.
- [49] H. Schulz, Gergely Ódor, Géza Ódor, and Máté Ferenc Nagy, Comp. Phys. Comm. **182**, (2011) 1467.
- [50] U. Dekker and F. Haake, Phys. Rev. **A11**, 2043 (1975)
- [51] E. Frey, U.C. Täuber, and T. Hwa, Phys. Rev. **E53**, 4424 (1996).
- [52] J. Kelling, G. Ódor, M. F. Nagy, H. Schulz, and K.-H. Heinig, The European Physical Journal - Special Topics, **210**:175-187, (2012).
- [53] M. Weigel, J. Comp. Phys., **231**(8):3064-3082, (2012).
- [54] NVIDIA CUDA Programming Guide, 3.1, (2010).
- [55] S. Gupta, S. N. Majumdar, C. Godrèche, and M. Barma, Phys. Rev. E **76**, 021112 (2007).
- [56] M. Krech, Phys. Rev. E **55**, 668 (1997)
- [57] M. Prähofer and M. Spohn, *In and Out of Equilibrium Progr. Probab.* No. 51 (Birkhäuser, Boston, 2002) pp 185-204